

ORNL/TM-2018/1081
CRADA/NFE-11-03264

Oak Ridge National Laboratory High-Strength, Lightweight Engines for Heavy-Duty Diesel Trucks



Approved for Public Release
CRADA Final Report for
CRADA Number NFE-11-03264

G. Muralidharan
M. P. Brady
A. Shyam
J. Qu
E. Cakmak
T. R. Watkins
J. A. Haynes
R. D. England
Y.-C. Chen
C. Trobaugh
H. Wang

December 20, 2018

DOCUMENT AVAILABILITY

Reports produced after January 1, 1996, are generally available free via US Department of Energy (DOE) SciTech Connect.

Website <http://www.osti.gov/scitech/>

Reports produced before January 1, 1996, may be purchased by members of the public from the following source:

National Technical Information Service
5285 Port Royal Road
Springfield, VA 22161
Telephone 703-605-6000 (1-800-553-6847)
TDD 703-487-4639
Fax 703-605-6900
E-mail info@ntis.gov
Website <http://www.ntis.gov/help/ordermethods.aspx>

Reports are available to DOE employees, DOE contractors, Energy Technology Data Exchange representatives, and International Nuclear Information System representatives from the following source:

Office of Scientific and Technical Information
PO Box 62
Oak Ridge, TN 37831
Telephone 865-576-8401
Fax 865-576-5728
E-mail reports@osti.gov
Website <http://www.osti.gov/contact.html>

This report was prepared as an account of work sponsored by an agency of the United States Government. Neither the United States Government nor any agency thereof, nor any of their employees, makes any warranty, express or implied, or assumes any legal liability or responsibility for the accuracy, completeness, or usefulness of any information, apparatus, product, or process disclosed, or represents that its use would not infringe privately owned rights. Reference herein to any specific commercial product, process, or service by trade name, trademark, manufacturer, or otherwise, does not necessarily constitute or imply its endorsement, recommendation, or favoring by the United States Government or any agency thereof. The views and opinions of authors expressed herein do not necessarily state or reflect those of the United States Government or any agency thereof.

Vehicle Technologies- Propulsion Materials

HIGH-STRENGTH LIGHTWEIGHT ENGINES FOR HEAVY-DUTY DIESEL TRUCKS

Author(s)
G. Muralidharan
M. P. Brady
A. Shyam
J. Qu
E. Cakmak
T. R. Watkins
J. A. Haynes
R. D. England
Y. C. Chen
C. Trobaugh
H. Wang

Date Published: December 2018

Prepared by
OAK RIDGE NATIONAL LABORATORY
Oak Ridge, Tennessee 37831-6283
managed by
UT-BATTELLE, LLC
for the
US DEPARTMENT OF ENERGY
under contract DE-AC05-00OR22725

Approved for Public Release

CONTENTS

LIST OF FIGURES	iv
LIST OF TABLES	v
ACKNOWLEDGMENTS	vi
ABSTRACT.....	1
1. STATEMENT OF OBJECTIVES	3
2. BENEFITS TO THE FUNDING DOE OFFICE’S MISSION.....	4
3. TECHNICAL DISCUSSION OF WORK PERFORMED BY ALL PARTIES.....	5
3.1 Exhaust Manifold.....	5
3.1.1 Oxidation Behavior [Reference to Brady Paper]	6
3.1.2 Constrained Thermal Fatigue Behavior [29]	9
3.1.3 Exhaust Manifold Casting and Testing	11
3.2 Pistons.....	12
3.2.1 Thermal Barrier Coatings [35].....	12
3.2.2 Lubrication Evaluation [51].....	14
3.3 Additively Manufactured compressor wheels.....	18
3.3.1 Background	18
3.3.2 Objectives and Tasks	18
3.3.3 Results.....	18
4. SUBJECT INVENTIONS	22
5. COMMERCIALIZATION POSSIBILITIES	23
6. PLANS FOR FUTURE COLLABORATION.....	24
7. CONCLUSIONS	25
8. REFERENCES	27
APPENDIX A. PUBLISHED PAPERS	A-3

LIST OF FIGURES

Figure 3.1. Oxidation data (100 h cycles) at 800°C in air with 10% H ₂ O	8
Figure 3.2. A schematic diagram and picture of the constrained thermal fatigue test	10
Figure 3.3. Constrained thermal fatigue lifetime of the six examined alloys. $T_{max} = 800^{\circ}\text{C}$;	11
Figure 3.4. Two-piece exhaust manifold fabricated using CF8CP stainless steel shows	11
Figure 3.5. Overall coating architecture used to prepare the thermal conductivity	13
Figure 3.6. Thermal diffusivity of sample A, C and F measured to 800°C.....	14
Figure 3.7. Three diesel pistons and one cylinder liner used in this study.....	15
Figure 3.8. Example of the coating wear and substrate wear for a polymer-graphite	16
Figure 3.9. Wear volumes of uncoated, polymer-graphite coated, and Mn-P	17
Figure 3.10. The calculated phase diagram for the Ti-48Al composition from the CALPHAD	19
Figure 3.11. A summary figure of the work completed on additive manufacturing.....	20
Figure 3.12. The powder particle size distribution of the sieved powder	21

LIST OF TABLES

Table 3.1. Components down selected and the critical materials properties of interest	5
Table 3.2. Typical compositions of cast alloys considered for used in exhaust manifolds.....	6
Table 3.3. Details of topcoat layers deposited on the specimens.	13
Table 3.4. Physical properties of the lubricants... ..	16
Table 3.5. Elemental composition of the Ti-48Al-2Cr-2Nb powder as obtained from wet chemical	21

ACKNOWLEDGMENTS

- Roman Pankiw from Duraloy Technologies, Inc. for providing cast austenitic stainless steels TMA 4705, TMA 6301, HP, and HK materials for study
- T. Lowe, M. Stephens, and G. Garner are thanked for their experimental work in evaluating oxidation resistance of various alloys
- S. Dryepondt, and B Pint for helpful comments and review
- Shane Hawkins, and Donald Erdman for their assistance with constrained thermal fatigue testing
- Dr. Donovan Leonard for Electron Microprobe and Wallace D. Porter at ORNL for thermo-physical property measurements
- Dr. Gopal Dwivedi and Prof. Sanjay Sampath of SUNY Stony Brook for thermal spray coatings
- Dr. G. Wu from Valvoline for providing the PC-11 diesel engine oils and their viscosities, R. J. Parten from Oak Ridge National Laboratory (ORNL) for sample preparation, and C. L. Roberts, an ORNL summer intern, for conducting a portion of the friction testing
- Dr. Dongwon Shin for his valuable contributions for the CALPHAD simulations
- Mr. Rick Lowden and Ms. Makayla Edwards for their help sieving the Ti-alloy powders
- Dr. Fred Montgomery is acknowledged for his assistance with the powder size distribution analysis
- Dr. Yukinori Yamamoto is acknowledged for valuable discussions regarding the phase transformation observed in Ti-alloy system

ABSTRACT

This project with Cummins supports the development of next generation heavy duty diesel engines that can achieve a 50% or better Break Thermal Efficiency (BTE). The fuel efficiency roadmap for the 50% BTE engine considers six main areas for efficiency improvement in the baseline engine, several of which involve making more efficient use of thermal energy (heat) in the engine. Increased operating temperatures and improved thermal management are expected to enable significant increases in *power density*, thus resulting in greater power output for the same sized engine or engine downsizing (or light weighting) for the same power output. However, it has become apparent that several key components will be exposed to temperatures beyond the capabilities of current engine and exhaust materials, requiring the availability of the next generation of high temperature materials to allow the engine to reach the targeted efficiencies, commercially viable durability, and emission targets. The objective of this project was to identify and/or develop key materials, and evaluate their critical properties to enable the design and development of a lightweight, higher efficiency engine, with enhanced temperature capability and reduced heat-loss to the atmosphere in order to facilitate waste heat recovery and improved efficiency.

An increase in the temperature capability of exhaust manifold materials, and piston materials were identified as having a positive influence on the efficiency of the next generation diesel engines. Since the current materials (High SiMo cast irons used in exhaust manifolds, and 4140 steel in pistons) are already operating near their limits of their temperature and strength capabilities, it was determined that new materials with the right combination of properties are required for these components.

Oxidation and constrained thermal fatigue tests were used to down-select CF8C plus (CF8CP), a cast austenitic stainless steel, for exhaust manifolds capable of operating at higher temperatures. A prototype exhaust manifold was fabricated using CF8CP and successfully tested in a marine engine. A functionally graded multiple-layer thermal barrier coating system was designed with four layers of mixed bondcoat alloy (NiCoCrAlYHfSi) and yttria stabilized zirconia (YSZ) and was shown to reduce the effective thermal conductivity of the coating-substrate (steel and Ti-6Al-4V) system. The graded alloy and YSZ mixture were intended to achieve better match of thermal expansion coefficient (CTE) and minimize thermal stresses. Such coatings can increase the temperature capability of pistons fabricated from steel and Ti-alloys.

Effect of oil additives and friction conformal contact friction tests showed there was a 15-30% reduction in friction by the polymer-graphite composite coating compared to the uncoated steel piston. Standalone Mn-P coating had little beneficial impact. Changing the oil from CJ-4 to PC-11 had little impact on the friction behavior in boundary lubrication. Wear behavior was tested under a point contact configuration with a high contact pressure. The candidate CK-4 oil showed similar or slightly better lubricity compared to the CJ-4 oil while the candidate FA-4 oil decisively increased the piston skirt wear. Although both coatings prevented scuffing failure observed for the uncoated steel skirt in a base oil without an additive package, they surprisingly caused a higher piston wear rate when tested in any of the fully formulated engine oil. The detrimental impact was attributed to the Mn-P film, either as a standalone coating, or a coating interlayer. The porous and brittle Mn-P film was broken during the wear test and the released hard Mn-P grains are suspected to cause third-body abrasion to accelerate the wear process.

This work also evaluated the feasibility of developing an improved high temperature, low mass, cost-neutral turbocharger compressor wheel for heavy-duty engine applications from TiAl using additive manufacturing, utilizing its unique ability to fabricate high strength, low weight structures. This work has shown that the phase transforming nature of the TiAl alloys enable obtaining equiaxed microstructures in the as-built state without the need for tedious beam parameter manipulations. The HIPed structures have good RT tensile properties that will enable them to be surface machined to the required tolerance that can

then be heat treated to obtain the desired microstructures. Additionally, the negligible residual stresses stemming from the high build chamber temperatures ensure the parts are formed without cracks (one of the major issues in traditional manufacturing of these intermetallics).

1. STATEMENT OF OBJECTIVES

This project with Cummins supports the development of next generation heavy duty diesel engines that can achieve a 50% or better Break Thermal Efficiency (BTE). The fuel efficiency roadmap for the 50% BTE engine considers six main areas for efficiency improvement in the baseline engine, several of which involve making more efficient use of thermal energy (heat) in the engine. Increased operating temperatures and improved thermal management are expected to enable significant increases in *power density*, thus resulting in greater power output for the same sized engine or engine downsizing (or light weighting) for the same power output. However, it has become apparent that several key components will be exposed to temperatures beyond the capabilities of current engine and exhaust materials, requiring the availability of the next generation of high temperature materials to allow the engine to reach the targeted efficiencies, commercially viable durability, and emission targets. Due to different combinations of property requirements, new materials technologies specific to the targeted engine components are needed to enable operation in the higher temperature environment.

The objective of this project was to identify and/or develop key materials, and evaluate their critical properties to enable the design and development of a lightweight, higher efficiency engine, with enhanced temperature capability and reduced heat-loss to the atmosphere in order to facilitate waste heat recovery and improved efficiency. This project was aimed at mitigating the risks and accelerating the use of advanced materials in the SuperTruck and subsequent high-efficiency diesel engines by developing cost-effective materials and processing techniques relevant to commercial engines. It was found that critical technologies such as waste heat recovery not only demanded the availability of improved materials to achieve the efficiency targets for the SuperTruck program in short-term engine efficiency measurements, but they will continue to drive the development of advanced materials to enable the manufacturing of a durable, commercially viable high thermal efficiency engine.

2. BENEFITS TO THE FUNDING DOE OFFICE'S MISSION

As outlined in the program website, the Vehicle Technologies Office (VTO) undertakes research and development activities to improve the efficiency of engines for both light and heavy-duty highway vehicles, whether they run on petroleum or alternative fuels. The office supports early-stage R&D to improve understanding of, and ability to manipulate, combustion processes, generating knowledge and insight necessary for industry to develop the next generation of engines that can be co-optimized with high performance fuels. VTO's research focuses on improving engine efficiency while meeting future federal and state emissions regulations through three main approaches:

- Developing advanced combustion strategies that maximize engine efficiency and minimize the formation of emissions within the engine cylinders
- Fuels effects research to develop better understanding how fuel properties and composition affect advanced combustion systems.
- Developing cost-effective aftertreatment technologies that further reduce exhaust emissions

Advanced materials are essential for boosting the fuel economy of modern automobiles while maintaining safety and performance. Because it takes less energy to accelerate a lighter object than a heavier one, lightweight materials offer great potential for increasing vehicle efficiency. A 10% reduction in vehicle weight can result in a 6%-8% fuel economy improvement.

This project with Cummins supports the development of next generation heavy duty diesel engines that can achieve a 50% or better Break Thermal Efficiency (BTE). The fuel efficiency roadmap for the 50% BTE engine considers six main areas for efficiency improvement in the baseline engine, several of which involve making more efficient use of thermal energy (heat) in the engine. Increased operating temperatures and improved thermal management are expected to enable significant increases in *power density*, thus resulting in greater power output for the same sized engine or engine downsizing (or light weighting) for the same power output. Development of new materials that can increase operating temperatures contribute to improved efficiencies and lightweighting, thus allowing the funding office to meet its program objectives.

3. TECHNICAL DISCUSSION OF WORK PERFORMED BY ALL PARTIES

A detailed analysis of the development of the high efficiency engine being envisioned by Cummins showed that a higher temperature capability in the exhaust system has significant impact on technologies that improve BTE by waste heat recovery from exhaust gases. In addition, an increase in the temperature capability of piston materials also had a positive influence on the efficiency of the next generation diesel engines. Since the current materials (High SiMo cast irons used in exhaust manifolds, and 4140 steel in pistons) are already operating near their limits of their temperature and strength capabilities, it was determined that new materials with the right combination of properties are required for these components. Replacement of current materials with materials with a higher strength and oxidation resistance at higher temperature also allows redesign of components to have thinner walls for the same stress levels, thus facilitating light-weighting and increased power density.

Table 3.1 shows the key properties that were initially identified by the team to be of interest for the two components. These properties were used for initial screening of new materials for this application and to define the initial test matrix.

Table 3.1. Components down selected and the critical materials properties of interest

Component	Critical Material Properties of Interest
Exhaust Manifold	Constrained thermal fatigue strength, elevated temperature strength, high temperature fatigue strength, creep strength, oxidation resistance, thermal expansion coefficient, specific heat, density, elastic modulus, thermal conductivity, microstructural stability at high temperatures, and the ability to be cast into complex shapes.
Piston	Constrained thermal fatigue strength, high temperature strength, high temperature fatigue strength, thermal conductivity, density, specific heat, oxidation resistance

In addition to exhaust manifolds, and pistons, an evaluation of additive manufacturing of Titanium Aluminide compressor wheels.

3.1 Exhaust Manifold

Several new classes of materials were identified as alternatives to the high SiMo cast irons currently used in exhaust manifolds. The following are the three major classes of materials:

1. D5S-austenitic nodular cast iron
2. Cast austenitic stainless steels (chromia-forming)
3. Alumina-forming, cast austenitic stainless steels.

Table 3.2 shows some example candidates of cast alloys being considered for this study. The “ORNL” in parenthesis shows that a particular class of alloy was developed at ORNL. Eight alloys of interest for exhaust components were considered for this study: a 4.1Si-0.7Mo-3.1C weight percent (wt.%) nodular ferritic SiMo cast iron, a 35Ni-4.7Si-2Cr-1.4C nodular austenitic D5S cast iron (comparable coefficient of thermal expansion, CTE, to SiMo), a 19Cr-12Ni austenitic CF8CP alloy [1,3], austenitic 25Cr/20Ni type cast HK and TMA 4705 [4-5] stainless steels, austenitic 25Cr/35Ni type cast HP and TMA 6301 stainless steels [6-7], and a developmental 14Cr-25Ni-3.5Al cast alumina-forming austenitic (CAFA) stainless

steel alloy designated CAFA 4 [8,9]. Analyzed compositions are presented in Table 3.2 (all compositions presented in wt.%).

Table 3.2. Typical compositions of cast alloys considered for used in exhaust manifolds

Alloy	Ni	Cr	Mo	Si	Al	Mn	Nb	V	W	Ti	Co	C	N	S	other
SiMo	0.01	0.02	0.7	4.1	0.01	0.24	-	-	-	0.04	-	3.13	32	40	0.02Cu 0.03Mg 0.015P
D5S	34.69	1.96	0.68	4.69	0.01	0.38	-	-	-	-	-	1.39	42	50	0.01Cu 0.03Mg 0.017P
CF8CP	12.50	19.27	0.35	0.45		3.43	0.83	0.07	0.02		0.09	0.075	2420	40	0.41Cu 0.02P
HK	18.14	25.57	0.05	1.68		0.93	0.19	0.02	0.07		0.07	0.47	490	70	0.06Cu 0.02P 0.01Ta
TMA 4705 (ORNL)	20.81	25.91	0.18	1.5	-	0.66	0.38	0.04	0.28	-	1.16	0.7	420	70	0.01Cu 0.01P
HP	34.17	25.48	0.04	1.61		0.63	1.14	0.04	0.24		0.1	0.42	611	30	0.05Cu 0.02P 0.001B
TMA 6301 (ORNL)	34.17	25.75	0.06	1.23	-	0.96	0.43	0.04	0.42	0.06	0.07	0.44	570	50	0.06Cu 0.022P
CAFA 4 (ORNL)	25.28	14.11	1.98	0.48	3.49	1.92	0.94	0.05	1.00	0.05	-	0.29	12	13	0.008B 0.51Cu 0.02P

3.1.1 Oxidation Behavior [Reference to Brady Paper]

Silicon-molybdenum (SiMo) cast irons are widely used for exhaust components, such as manifolds and turbocharger housings, in automotive and heavy-duty truck diesel engine applications [10-15]. However, the increased operating temperatures are expected to push SiMo cast iron properties such as strength, fatigue, and oxidation beyond their acceptable limits. A number of studies of the high temperature oxidation behavior of SiMo cast irons, in some cases in comparison to advanced cast irons, cast ferritics, and/or cast austenitics, under conditions relevant to exhaust systems have recently been reported [12-21]. However, these studies have focused on mechanistic aspects and characterization after relatively short - term oxidation exposures (generally < 500 h). The goal of the present work was to complement the existing literature by investigating the long-term oxidation resistance (5000 h total) of a series of candidate next generation exhaust component alloys relative to SiMo cast iron in the temperature range of 650-800°C. The exposures were conducted in an aggressive laboratory test condition of air with 10 volume % water vapor, as exhaust gases contain water vapor (typically 2-12% for diesel exhaust [22]), and water vapor is frequently linked with significant degradation in oxidation resistance, particularly for Cr-containing alloys [23,24].

The oxidation behavior of candidate cast alloys for diesel engine exhaust components was studied for up to 5000 h at 650, 700, 750, and 800°C in air with 10% H₂O. The SiMo, D5S, HK, TMA 4705, HP, TMA 6301, and CF8CP samples were electro discharge machine (EDM) cut from commercial castings, and the CAFA 4 EDM cut from a 0.5 kg range laboratory vacuum arc-casting. Oxidation test samples ~20 mm x 10 mm x (1-1.5) mm were polished to a 600 grit USA finish using SiC polishing papers. Oxidation exposures were conducted in 100 h cycles at 650, 700, 750, and 800°C with mass changes measured after every cycle (air cooling). Oxidation in air with 10 vol. % water vapor was conducted by flowing air through an alumina tube inside a resistively heated tube furnace [25]. Distilled water was added by

atomization into the flowing gas stream above its condensation temperature. Test samples were positioned in alumina boats in the furnace hot zone so as to expose the specimen faces parallel to the flowing gas.

The SiMo and D5S cast irons exhibited several orders of magnitude faster oxidation than the chromia- and alumina- forming austenitics under all conditions studied. Such behavior is expected, and consistent with their very low Cr contents and dependence on modest levels of Si for oxidation resistance (Table 3.2). At 650°C in air with 10% H₂O, the D5S exhibited moderately lower oxidation kinetics than the SiMo cast iron, with mass change of ~50 mg/cm² for SiMo and ~30 mg/cm² for D5S after 5000 h and little to no oxide scale spallation evident. However, at 700 and 750°C in air with 10% H₂O, the D5S suffered from oxide scale spallation and mass loss in the first few hundred hours of exposure, whereas the oxide scale formed on the SiMo cast iron remained adherent despite specific mass gains (mass change normalized by initial, unoxidized sample surface area; referred to only as “mass change” in remainder of text for simplicity) of nearly 100 mg/cm² at 700°C. Because of this susceptibility to oxide scale spallation, the D5S was not evaluated at 800°C.

The SiMo cast iron exhibited an unusual pattern of oxidation mass change behavior with increasing temperature. The extent of oxidation increased from 600°C to 700°C but the extent of oxidation for SiMo at 750°C in air with 10% H₂O was lower than at 700°C. At 800°C in air with 10% H₂O, the oxidation of SiMo was significantly lower up to 3000 h of exposure, at which point the oxidation increased. No significant mass loss or scale spallation was observed for the SiMo under all conditions studied.

The pattern of oxidation behavior for the chromia-forming austenitics trended with the level of Cr and Ni additions in these alloys. At 800°C in air with 10% H₂O (Fig. 3.1), the lowest Cr and Ni alloy, CF8CP with ~19Cr and ~12Ni (Table 3.1), exhibited extensive mass loss and scale spallation (~-60 mg/cm² at 2000 h of exposure) consistent with rapid, nonadherent Fe-oxide base scale formation. In contrast, good oxidation resistance with only modest mass loss behavior (0 to -1 mg/cm² range) consistent with chromia volatilization was observed for the first 2500 h of exposure for the ~20Ni-25Cr class HK and TMA 4705 alloys, and the ~35Ni-25Cr HP and TMA 6301 alloys. The HK alloy exhibited a transition to Fe-oxide scale formation and spallation from ~2500-5000 h of exposure, whereas the TMA 4705, HP, and TMA 6301 continued to exhibit only modest mass loss behavior (all less than -3 mg/cm² after 5000 h at 800°C).

Modest mass loss consistent with chromia volatilization [26, 27] was generally observed for HK, TMA 4705, HP, and TMA 6301 from 650-750°C. At 700 and 750°C, the lower Cr/Ni CF8CP continued to show relatively lesser oxidation resistance consistent with a transition to Fe-oxide formation and spallation (CF8CP was not evaluated at 650°C in air with 10% H₂O). In contrast, the developmental alumina-forming alloy CAFA 4 generally showed excellent oxidation resistance and small positive mass gains (less than 1 mg/cm²) from 700-800°C for the 5000 h test period. For further details, please refer to [28].

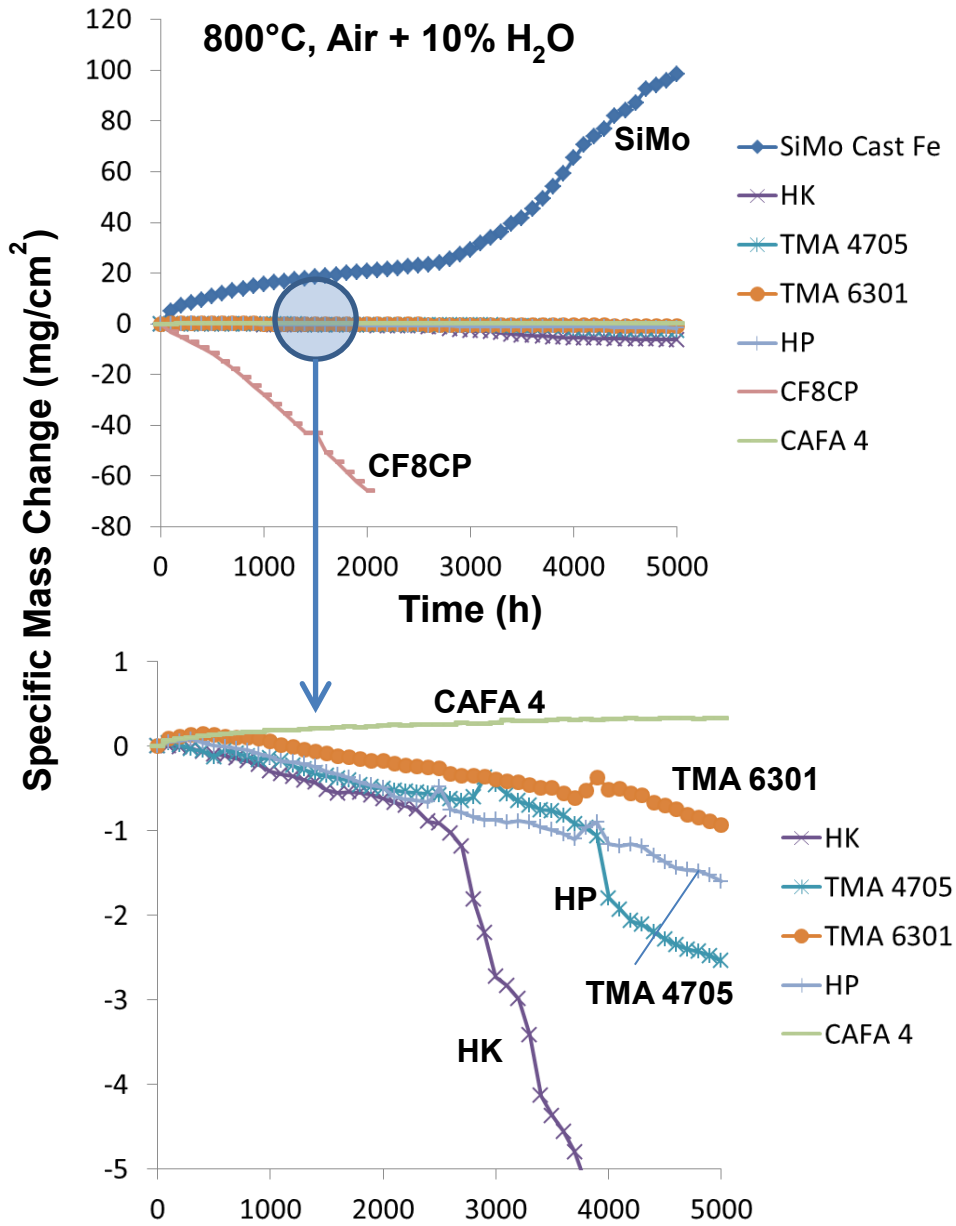


Figure 3.1. Oxidation data (100 h cycles) at 800°C in air with 10% H₂O. Same data, two different specific mass change scales. The mass change data for CAFA 4, HP, and HK are from reference 9.

The oxidation behavior of the alloys are summarized below [28].

- 1) The alloys in order of oxidation resistance from best to worse were: alumina-forming CAFA 4 > chromia-forming 35Ni-25Cr type TMA 6301 and HP > 25Ni-25Cr type TMA 4705 > 25Ni-25Cr type HK > 19Cr-12Ni CF8CP > SiMo and D5S.

- 2) Oxide scale spallation issues were observed for D5S from 700-750°C. SiMo exhibited moderately faster oxidation than D5S, but the scales remained relatively adherent despite reaching hundreds of microns in thickness under some conditions. These results suggest that D5S may not be a good alternative to SiMo to achieve higher operating temperatures in exhaust applications for designs where spalled oxide particles may damage downstream components.
- 3) Accelerated oxidation in water vapor was observed for the 19Cr-12Ni CF8CP from 700-800°C, with Fe-oxide formation and extensive scale spallation observed.
- 4) Accelerated oxidation and/or water vapor volatility driven Cr loss was not a major issue for the 25Ni-25Cr chromia-forming austenitics up to 750°C, and the 35Ni-25Cr chromia-forming austenitics up to 800°C (highest temperature studied). These alloys exhibited good oxidation behavior out to the 5000 h test duration studied, with EPMA line scans of Cr levels near the oxide-alloy interface suggesting that the good oxidation resistance may be maintained for longer periods. A concern for this class of alloys was internal attack of second phases at alloy austenitic matrix grain boundaries, which may lead to degradation in strength and/or thermal fatigue characteristics.
- 5) The developmental family of cast alumina-forming austenitic steels offer potential for improved oxidation resistance in exhaust environments. Their adoption (as well as the potential adoption of chromia-forming austenitics) will depend on their weldability, castability and exhaust system design suitability, particularly with regards to thermal conductivity and expansion properties that determine the thermal fatigue resistance in service.

3.1.2 Constrained thermal fatigue behavior [29]

Constrained thermal fatigue (CTF) is a common cause of failure in automotive and heavy-duty diesel engine components. CTF loading involves cycling of temperature superimposed on mechanically constrained components such as exhaust manifolds and engine cylinder heads [30]. While models to determine the isothermal low cycle fatigue performance are well established (e.g. Coffin-Manson model), similar models for constrained thermal fatigue are material specific and invariably require extensive numerical and finite element computations [30-33]. Direct evaluation and ranking of the constrained thermal fatigue performance of materials, moreover, remains a challenge [34]. In this work, A setup was developed to evaluate the constrained thermal fatigue performance of alloys.

The test specimens were rigidly constrained in this testing methodology, in a servohydraulic test machine in displacement control (Fig. 3.2), and cyclic stresses were generated by temperature cycling in the gage section of the specimen between specified temperatures and at a specified heating rate. Heating of specimens was achieved by combining several resistance heaters. In addition, a hold time at the maximum temperature in the cycle was introduced to generate a trapezoidal temperature versus time control signal. All the reported tests in the present investigation had a maximum temperature of 800°C and hold time at maximum temperature of 60 seconds. Heating/cooling rates of 1°C/second were employed in the reported tests with a feedback loop temperature controller (with Proportional Integrative Derivative, PID control). Precise temperature control (less than 5°C variation) in the gage section of the specimen was achieved by a Labview® software code. A high temperature extensometer was placed in the gage section of the specimen and the evolution of the stress and strain signals with thermal cycling was continuously recorded. The performance of six cast ferrous alloys was evaluated in constrained thermal fatigue loading conditions. Three cast irons were examined namely a SiMo cast iron (referred to as SiMo), a high SiMo cast iron (high SiMo) and a Ni-resist cast iron (D5S). The CTF performance of three cast austenitic stainless steels, namely CF8CP, TMA 4705 and TMA 6301, was also examined. The specimens were cycled to failure. The fracture surfaces of selected specimens was examined by scanning electron microscopy (SEM).

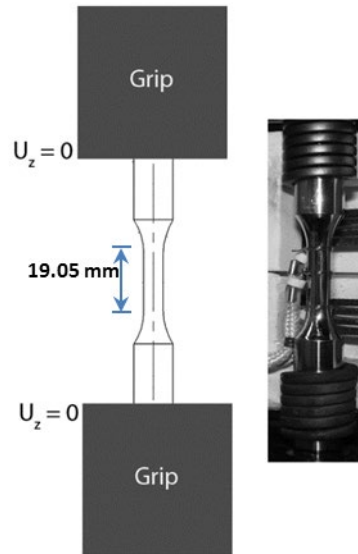


Figure 3.2 1

Figure 3.2. A schematic diagram and picture of the constrained thermal fatigue test specimen.

The CTF test performance of the six examined cast ferrous alloy is summarized in Fig. 3.3. The maximum temperature for the reported tests was 800°C with heating cooling rates of 1°C/sec and a hold time of 60 seconds at the maximum temperature. Arrows in Fig. 3.3 indicate runout specimens, where the tests were terminated prior to failure.

It can be observed in Fig. 3.3 that as the temperature range (ΔT) is increased, the failure lifetime decreased. This is due to the fact that under the constrained conditions, an increase in ΔT directly corresponds to an increase in the stress range during temperature cycling. The temperature in Fig. 3.3 can, therefore, be considered to be analogous to stress in S-N curves generated by isothermal load controlled tests. The results in Fig. 3.3 indicate that at high values of ΔT , failure can occur in less than 10 cycles whereas thousands of cycles are required at a ΔT value of 100°C.

Power law fits to the data for the six alloys are also included in Fig. 3.3. Other than D5S, the fits are reasonably good for the other five alloys. The Ni-resist alloy D5S displayed unusually short CTF lifetimes at intermediate ΔT values of 225-250°C. In general, it can be concluded from Fig. 3.3 that the alloys that have curves with longer lifetime at the same ΔT have higher CTF resistance. Accordingly, the higher CTF resistance alloys have longer CTF lifetimes at the same value of ΔT and/or an increased tolerance for a higher ΔT at a given CTF lifetime. As such, the cast austenitic steels display better CTF performance than the cast irons in Fig. 3.3. The CTF performance of the six alloys examined can be ranked on the basis of results in Fig. 3.3 as follows (best to worst): CF8CP > TMA6301 > TMA4705 >> D5S > High SiMo ~ SiMo cast iron. For further details, please refer [29].

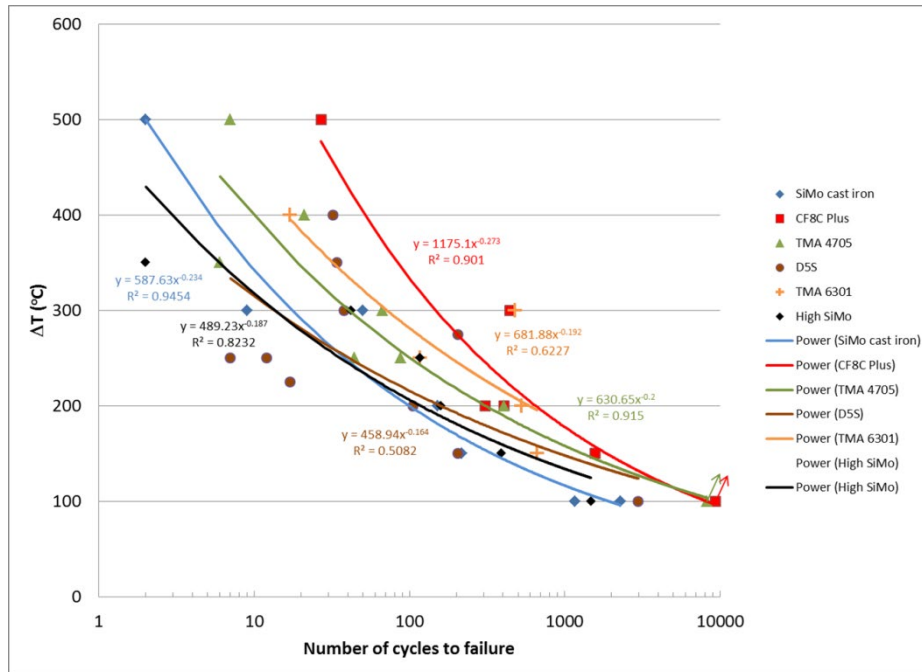


Fig. 3.3. Constrained thermal fatigue lifetime of the six examined alloys. $T_{max} = 800^{\circ}\text{C}$; hold time = 60 seconds; heating/cooling rate = $1^{\circ}\text{C}/\text{second}$.

3.1.3 Exhaust manifold casting and testing

Based upon the oxidation and constrained thermal fatigue properties, CF8 plus was down-selected for fabrication and testing of prototype exhaust manifold. MetalTek International cast two-piece prototype exhaust manifolds out of CF8CP stainless steel. One set of manifolds was engine-tested for endurance in a severe marine cycle for 500h and performed well. Figure 3.4 shows images from the two-piece exhaust manifold that was tested under severe conditions. Although there is some evidence of mild external oxidation, the manifolds show excellent integrity. Based upon these results, Cummins is considering CF8CP cast stainless steel for use in commercial applications.



Figure 3.4. Two-piece exhaust manifold fabricated using CF8CP stainless steel shows good integrity after engine testing.

3.2 Pistons

Two broad areas of research were pursued as part of this work were pursued as part of this project:

1. Thermal barrier coatings to reduce the temperatures experienced by the pistons
2. Evaluate the effect of lubricants on reducing friction between piston and cylinder walls

3.2.1 Thermal Barrier Coatings [35]

Ceramics coatings have long been used as thermal barriers for aircraft and automobile engines operating at high temperatures [36, 37]. Thermal barrier coatings (TBCs) allow the engine gas temperatures to significantly exceed the limits of traditional alloys or steels, which benefits engine efficiency, and in some cases, emissions [38]. Many studies have focused on lowering the thermal conductivities of the coatings, while still maintaining good thermo-mechanical integrity [39-40]. Besides lowering thermal conductivity by doping heavy elements for phonon scattering, multiple layer TBCs have been used to increase interface scattering of the phonons and oxidation resistance [40]. For example, alternate YSZ and YAG layers were used to promote interface scattering [39].

Initial applications of TBCs on diesel engines were carried out using a Cummins V903 direct injection engine under DOE/NASA and TACOM programs [41] focusing on cylinder head and piston coatings. The TBC is designed as a thermal shield, with the goal of ultra-low thermal conductivity. But this reduced thermal conductivity can also be a source of high thermal stresses, particularly in thicker coatings. Although TBCs have been used to protect internally-cooled stationary and rotating hot section components in aero engines for decades, introduction of TBCs into high volume reciprocating engines has been a very slow process due to the extreme conditions on the piston crown surface and the very long service lives of heavy duty diesel engines prior to first overhaul [41-43]. On the other hand, TBCs have been widely used in race car engines in which short term performance is more important than long term durability [44]. Improving the thermo-mechanical properties of the TBC system, while maintaining or improving thermal resistance, is a key for commercial TBC application in diesel engines.

A typical TBC system for aircraft applications consists an alloy (Ni-base super alloy) substrate coated with a bondcoat (MCrAlY) and then a ceramic top coating (e.g. 8YSZ). A thermally sprayed bondcoat provides oxidation resistance to the substrate, a roughened surface for mechanical bonding of the ceramic top coat, and may also provide a buffer region to transition from alloy to ceramic. However, there is still a clear boundary between the bondcoat and TBC which forms thermally grown oxides (TGO) due to oxidation of the bond coat during high temperature exposure. This oxidized interface is a major contributor to delamination failure of the ceramic top coat and remains a weak link for TBCs. The cyclic nature of piston strokes in a reciprocating engine adds high frequency thermomechanical stresses to the coating. A simple substrate-bond-coat-TBC system will not typically survive these conditions to achieve long term engine service life for commercial vehicles.

In this work, a functionally graded coating system with gradual transition from bondcoat to ceramic coating was used in order to better accommodate thermal stresses. In the present study, a multiple-layer coating system was designed with four layers of mixed bondcoat alloy (NiCoCrAlYHfSi) and yttria stabilized zirconia (YSZ) with thicknesses of 100 μm , 50 μm , 50 μm and 700 μm . The graded alloy and YSZ mixture were intended to achieve better match of thermal expansion coefficient (CTE) and minimize thermal stresses. In this study, we evaluated the thermal transport properties of the multiple-layer system and its microstructure.

Thermal barrier coatings were prepared at the Thermal Spray Laboratory at SUNY Stony Brooks using an air-plasma spray system. To evaluate thermal conductivity of various coating architectures, coatings were deposited on the flat surface of 12.7 mm diameter discs with 15 mm thickness. Three different substrate

materials were selected for this study, Ti-6Al-4V, 4140 steel and graphite. Graphite was used to prepare free-standing coating by grinding off the soft substrate material. In order to improve coating adhesion, the metal substrate surfaces were grit-blasted at a pressure of 4 bar using Al₂O₃ grit, which resulted in surface roughness of ~3.5 μm Ra. The substrates were then immersed in isopropanol solution followed by ultrasonication for 10 minutes, to remove any grit residue and contamination. All the coatings were deposited via atmospheric plasma spray process using an F4MB™ (Oerlikon Metco, Westbury, NY, USA) spray torch. Each coating architecture consisted of a 150 μm bondcoat layer of NiCoCrAlYHfSi (Amdry 386-2, Oerlikon Metco, Westbury, NY). The top coat for each coating contained four layers, TC1, TC2, TC3 and TC4. Each layer utilized an incremental mixture of NiCoCrAlYHfSi and yttria-stabilized zirconia (YSZ, SG 204, Saint Gobain Ceramics, Worcester, MA, USA). The details of each layer's metal/ceramic mixture and the associated processing conditions are shown in Figure 3.5 and Table 3.3.

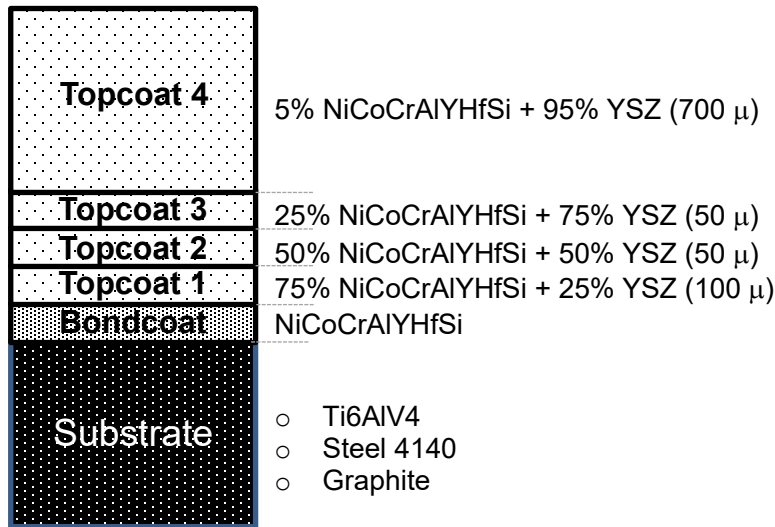


Figure 3.5: Overall coating architecture used to prepare the thermal conductivity specimen.

Table 3.3: Details of topcoat layers deposited on the specimens. Specimens A to F had 150μm bondcoat layer. G-H were freestanding specimens after removing the graphite.

Specimen ID	Substrate	TC1 (~100μm)	TC2 (~50μm)	TC3 (~50μm)	TC4 (~700μm)	Total target Coating Thickness (μm)
A	Ti-6Al-4V					0
B	Ti-6Al-4V	X	X	X		200
C	Ti-6Al-4V	X	X	X	X	900
D	4140					0
E	4140	X	X	X		200
F	4140	X	X	X	X	900
G	Graphite	X				100
H	Graphite	X	X			150
I	Graphite	X	X	X		200
J	Graphite	X	X	X	X	900

Thermal diffusivity of the coatings was measured using two flash diffusivity systems: a TA Instrument Flashline5000 and a Netzsch FLA457 Microflash. The samples were 12.7 mm in diameter. Substrates

were 1.5 mm thick and the total coating thicknesses were from 0.2 mm to 0.9 mm. Standard thermal diffusivity testing following ASTM 1461-2009 was performed using classic analysis [45-48]. Specific heat (C_p) was measured using a Netzsch 404C Pegasus differential scanning calorimeter (DSC) following ASTM 1269 [49] from room temperature to 800 °C at 20 °C/min heating and cooling rate. Samples are about 5.5 mm in diameter. For thin samples, up to 4 disks were used to make the total mass between 130-150 mg. For all samples, thermal diffusivity (α), the average density (ρ) of the layers and C_p of the layered mixture were used to calculate thermal conductivity, κ :

$$\kappa = \alpha\rho C_p \quad (1)$$

Coating sprayed on graphite spalled off due to thermal expansion mismatch during cooling after thermal spray and the remaining graphite was ground off. Thus, samples G, H, I and J from Table 3.3 were used as freestanding coatings. Samples A, C and F were substrates and coatings on substrates.

Two coatings with the full thickness of all layers, C and F, were tested with the Ti-6Al-4V and 4140 steel substrates, respectively. As shown in Figure 3.6, the effective thermal diffusivities of the two samples (C and F) were lowered significantly by the TBCs (when compared to the substrate A), and exposure at 800°C did not show significant sintering and no hysteresis was detected after measurements at 800°C. It should be noted that the thermal diffusivity values are only related to the 1 mm thick substrate and the 900 μm TBC. The thermal conductivity of the graded TBC has a room temperature values of 1.2 W/mK and decreases slightly at high temperatures. It is comparable to the TBCs based on YSZ [50]. In fact, the mixing of 5 vol% bondcoat with 95% YSZ in the final layer showed thermal conductivity was reduced by the additional alloy phase.

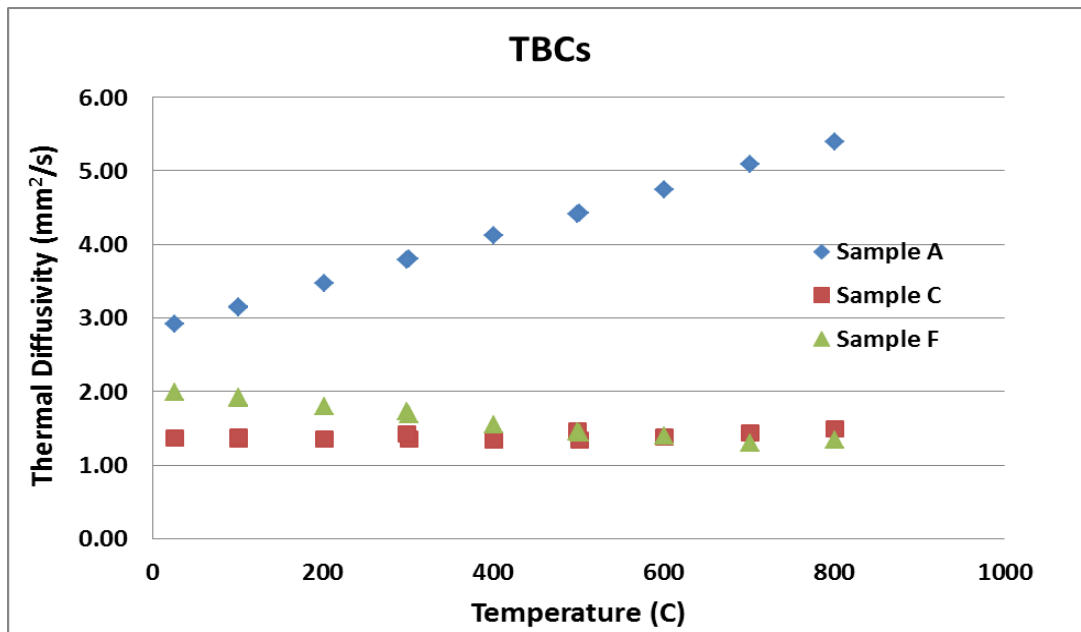


Figure 3.6. Thermal diffusivity of sample A, C and F measured to 800°C.

3.2.2 Lubrication evaluation [51]

Roughly 10-15% of total energy generated in an internal combustion engine is lost to parasitic friction [52]. In the piston-cylinder assembly, while the piston rings may account for more than 70% of the total

friction-induced energy losses [51], the piston skirt contribution to the friction of the system could also be substantial [54-56] and should not be overlooked. Other researchers have stressed that the friction between the piston skirts and cylinder walls could even be comparable in magnitude to the friction between the rings and the cylinder walls in certain circumstances [57,58]. Coating the piston skirts [59,60] is among the materials approaches for reduction of friction, noise, and scuffing, particularly to address the increasing peak-cylinder-pressure and decreasing oil viscosity in heavy-duty diesel engines.

Manganese phosphate (Mn-P) coatings have been used in industry for more than half a century for anti-scuffing/anti-seizure and wear protection in both dry and lubricated environments, but the literature on their tribological behavior is surprisingly limited, with only a little more than a dozen of reports found in our survey [61-73].

In this work, three diesel piston skirts, one uncoated steel, another coated with a standalone Mn-P film, and the third coated with a polymer-graphite composite layer on top of a Mn-P interlayer, were tribologically investigated in a base oil without additives, a commercial API CJ-4, and two candidate PC-11 diesel engine oils, as well as in an additive-free basestock.

Three diesel pistons were provided by Cummins: (1) uncoated 38MnSiVS5 steel, (2) skirt coated with a Mn-P film, and (3) skirt coated with a polymeric matrix containing colloidal graphite short fibers, and a Mn-P interlayer (henceforth referred to as polymer-graphite coating). The photographs of the three pistons are shown in Figure 3.7.

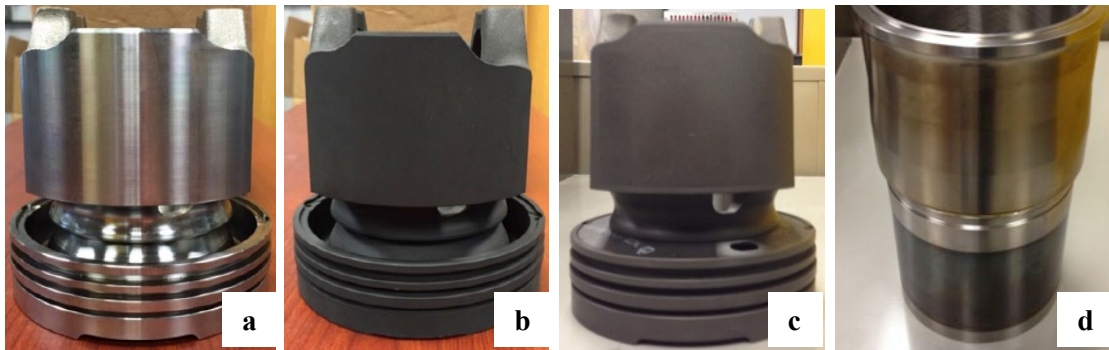


Figure 3.7. Three diesel pistons and one cylinder liner used in this study. (a) Uncoated steel piston, (b) Piston with a Mn-P coating, (c) Piston with a polymer-graphite coating, and (d) Cast iron cylinder liner.

Tribological tests were carried out on a reciprocating tribometer (Plint TE77, Phoenix Tribology Ltd.) with a piston skirt specimen (9.5x9.5 mm sectioned out using wire electrical discharge machining) sliding against a 25x25 mm square section of the cylinder liner. Two different sample configurations were used. Conformal contact between the skirt and liner, in the same orientation as in an actual engine, was used to measure the friction at a contact pressure in the range of that in an operating engine. Point contact was realized by flipping the cylinder liner coupon (polished using 180 grit SiC abrasive paper) and turning the piston skirt coupon by 90° to create a high contact pressure to accelerate the wear process. The tests in both the conformal and point-contact configurations were performed under a 240 N normal load at an oil temperature of 100°C. The oscillation frequency used was 10 Hz with a stroke length of 10 mm, with a total sliding distance of 1000 meters. At least two repeat tests were conducted for each material in each testing condition. The contact pressure in the conformal contact falls in the range of that in an engine, and the point contact provides a much higher contact stress. The worn samples were ultrasonically cleaned before the wear quantification using an optical interferometer (Wyko NT9100). For a coated surface, the

material loss of the coating was subtracted from the total wear volume, so as to allow direct comparison of the wear of the steel substrate to that of the uncoated piston. Figure 3.8 shows an example, illustrating the total wear, the coating wear, and the substrate wear for a polymer-graphite coated piston skirt specimen.

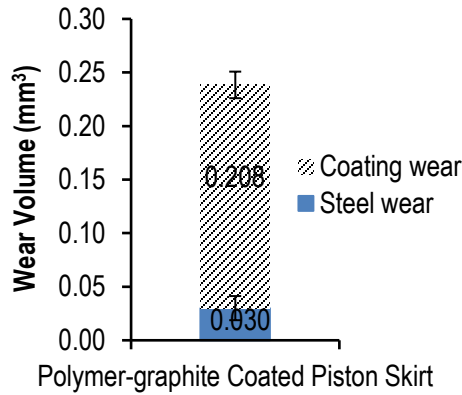


Figure 3.8 Example of the coating wear and substrate wear for a polymer-graphite coated piston skirt specimen.

Four different lubricants were provided by Valvoline and used in this study: three fully-formulated diesel engine oils, a commercial mineral-synthetic blend CJ-4, a candidate mineral-synthetic blend CK-4 (PC-11a), and a candidate fully-synthetic FA-4 (PC-11b), and the base oil for CJ-4 without the additive package. Table 3.4 shows the densities and viscosities of the four lubricants.

Table 3.4 Physical properties of the lubricants

Lubricant	Density (g/cc)	Viscosity @ 100°C (cSt)	Viscosity @ 40°C (cSt)
CJ-4	0.88	14.0	107.6
CK-4 (PC-11a)	0.86	9.9	64.3
FA-4 (PC-11b)	0.86	10.1	55.1
Base oil for CJ-4	0.86	6.4	45.0

Figure 3.9 compares the wear volumes of the steel substrates for the three piston skirts in the three fully-formulated diesel engine oils. For the uncoated piston, the candidate CK-4 protects the surface well with even less wear than the conventional CJ-4, despite lower oil viscosity. In contrast, the candidate FA-4 did not do as well with more than double the wear compared with the CJ-4. Results suggest that while the CK-4 seems to be a suitable low-viscosity replacement for the CJ-4, the FA-4 oil may induce a potential wear challenge.

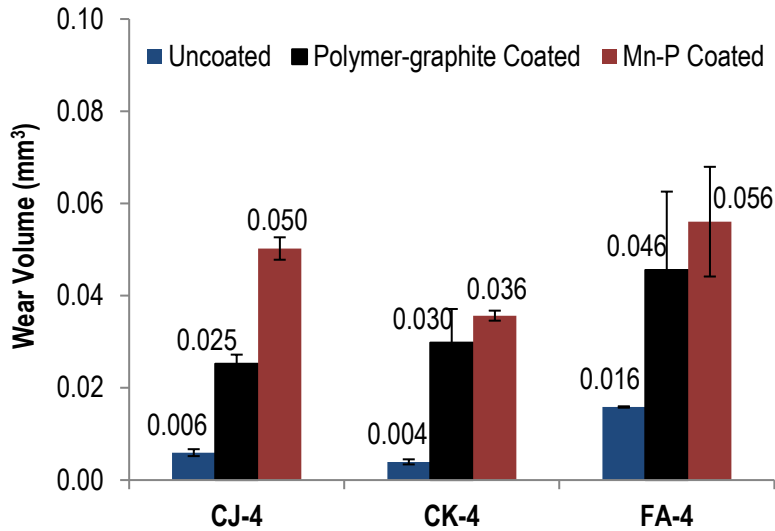


Figure 3.9. Wear volumes of uncoated, polymer-graphite coated, and Mn-P coated piston skirts tested in fully-formulated CJ-4 and candidate PC-11 engine oils.

It was surprising that both the skirt coatings, instead of providing a wear protection, increased the material loss of the steel piston substrate (after subtracting the material loss of the coatings themselves). The polymer-graphite coating increased the wear of the steel substrate by 3-7 times, while the Mn-P coating was even worse making the steel substrate worn 4-9 times faster! It was hypothesized that the wear particles from the broken Mn-P coating were basically hard Mn-Fe orthophosphate grains and acted as abrasive at the contact interface to induce third-body abrasion to accelerate the wear of the piston steel substrate [51]. The polymer-graphite coating has a Mn-P interlayer and experienced the same third-body abrasion problem when the top coat was worn through to expose the interlayer to contact and rubbing. The porous and brittle Mn-P coating is beneficial in harsh rubbing contact conditions or poor lubricants by separating the two metal surfaces to avoid severe adhesion or scuffing failure, allowing fast running-in, and retaining oil. On the other hand, the Mn-P coating could detrimentally accelerate the sliding wear rate by releasing hard Mn-Fe orthophosphate grains to promote third-body abrasion in certain well-lubricated, high contact pressure conditions.

In summary, conformal contact friction tests showed there was a 15-30% reduction in friction by the polymer-graphite composite coating compared to the uncoated steel piston while the standalone Mn-P coating had little beneficial impact. Changing the oil from CJ-4 to PC-11 had little impact on the friction behavior in boundary lubrication. Wear behavior was tested under a point contact configuration with a high contact pressure. The candidate CK-4 oil showed similar or slight better lubricity to the CJ-4 oil while the candidate FA-4 oil decisively increased the piston skirt wear. Although both coatings prevented scuffing failure observed for the uncoated steel skirt in a base oil without an additive package, they surprisingly caused a higher piston wear rate when tested in any of the fully formulated engine oil. The detrimental impact was attributed to the Mn-P film, either as a standalone coating, or a coating interlayer. The porous and brittle Mn-P film was broken during the wear test and the released hard Mn-P grains are suspected to cause third-body abrasion to accelerate the wear process.

3.3 ADDITIVELY MANUFACTURED COMPRESSOR WHEELS

3.3.1 Background

Titanium Aluminide (TiAl) is an intermetallic alloy with high specific strength, good corrosion/oxidation resistance at relatively high temperatures, and excellent strength retention until the brittle ductile transformation temperature ($\sim 800^\circ\text{C}$). Recently there has been increased interest in using TiAl for the manufacture of high temperature engineering components such as gas turbine blades and turbocharger components. However, its brittle nature at low temperatures makes it difficult to machine into complex shapes. Additive manufacturing (AM) holds the potential to revolutionize the manufacturing of such intricate components from this brittle alloy.

3.3.2 Objectives and tasks

The objective of this work was to develop an improved high temperature, low mass, cost-neutral turbocharger compressor wheel for heavy-duty engine applications using additive manufacturing, utilizing its unique ability to fabricate high strength, low weight structures.

The major tasks of this task were as-follows:

1. Perform detailed computational thermodynamic analyses to understand the solidification mechanisms
2. Adjust the powder size distribution to the required specifications
3. Perform elemental analysis of the Ti-48Al-2Cr-2Nb powder
4. Print the prototype compressor wheel

3.3.3 Results

The calculated phase diagram and Scheil simulations for the Ti-48Al-2Cr-2Nb (at%) alloy are presented in Figure 3.10. Based on the composition indicated with the right dotted line (labelled 1wt% Al loss) on the phase-diagram in Figure 3.10a, the solidification path is expected to start in the BCC-B2 phase (L+B2) field. As experimentally observed and verified with the calculated phase diagram, the as-solidified structure consists of the ordered FCC γ -TiAl and ordered HCP α_2 -Ti₃Al phases. As Figure 3.10a shows, γ and α_2 phases govern the phase stability of Ti-Al binary at the composition range between the dotted lines labelled Ti-48Al (at%) and 1wt% Al loss due to evaporation (Ti-47.3Al) upon equilibrium cooling. Further, the precipitation of α_2 -Ti₃Al is promoted as the relative amount of Ti increases by losing Al during the EBM process (a total of 1 wt.% Al loss was documented with wet chemical analysis).

The Scheil simulations (Figure 3.10b and c) are used to predict the solidification sequence under non-equilibrium solidification conditions (closer to AM conditions). Both binary (Ti-48Al) and quaternary (Ti-48Al+Nb/Cr) systems, with the composition to replicate experimentally observed 1 wt.% loss of Al, are used (i.e., Ti-47.3Al and Ti-47.2Al-2Nb-2Cr, respectively). Here Figure 3.10b shows the solidification sequence from the liquid phase whereas Figure 3.10c shows the formation range of the γ and α phases. The Scheil simulations are performed down to around 1350 °C which remains in the γ + α regime. For example, as to how Figures 3.10b and c correspond, the TiAlNbCr (Scheil) curve in Figure 2b indicates that α phase solidification starts at $\sim 1505^\circ\text{C}$. Points WW and UU in Figures 3.10b and c, respectively, correspond indicating that only α phase is precipitating out of the liquid. This continues to points XX and YY & TT, respectively, wherein the γ phase starts to precipitate out of the liquid as well. Thus, both γ and α phases precipitate out of the liquid following curve segments XX-ZZ and YY-SS & TT-VV. Note that the α phase is circled with red in Figure 3.10a in the equilibrium phase diagram. The α_2 phase forms from the α through a solid-state phase transformation. A similar approach can be used to interpret the TiAl (Scheil) binary curves.

Overall, the Scheil simulations predict that the solidification starts with the α phase which then is joined by γ . Intriguingly, the addition of Nb and Cr affects the profile of binary Ti-48Al cooling particularly at the later stage as shown in Figure 3.10b. While the binary Ti-48Al has a plateau in the ternary eutectic ($L+\alpha+\gamma$), that of modified quaternary extends over a much wider temperature range. The difference is attributed to the formation of γ over a wide temperature as shown in Figure 3.10c in the case of the quaternary.

These results support our hypothesis that the complex solidification path that starts in the $L+B2$ phase field and ends in the $\gamma + \alpha_2$ phases and effectively breaks the epitaxial growth during the deposition, due to having different crystal structures. The numerous phase transformations during solidification and subsequent heating further refine the microstructure. Additionally, since these microstructures are phase transformation driven, they are expected to be relatively part geometry-independent.

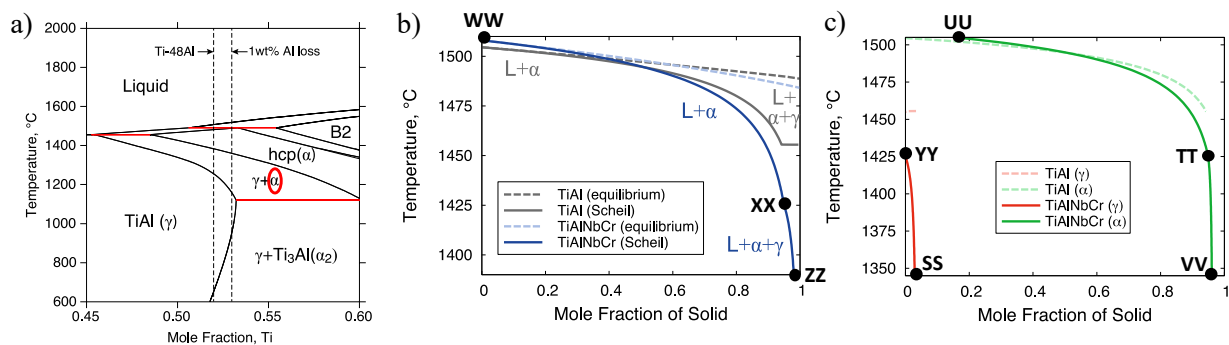


Figure 3.10. a) The calculated phase diagram for the Ti-48Al composition from the CALPHAD simulations, b) The Scheil simulation showing the solidification sequence for Ti-48Al and Ti-48Al-2Cr-2Nb compositions and c) The Scheil simulation showing the formation range of the γ (TiAl) and α phases for Ti-48Al and Ti-48Al-2Cr-2Nb compositions. The α phase circled with red in (a) corresponds to the α phase in (b) and (c).

Using this information, Ti-48Al-2Cr-2Nb preforms have been successfully manufactured using the ARCAM Electron Beam Melting (EBM) technique using standard build parameters. Hot Isostatic Pressing (HIP) was employed to eliminate pores and homogenize the microstructures, post-manufacture. XRD residual stress measurements revealed negligible residual stresses in the as-built parts as expected from the high temperature of the powder bed during the build. XRD phase-ID measurements revealed two-phases with the matrix γ -TiAl and the precipitate Ti_3Al (α_2) phases. The presence of these phases was confirmed with the EBSD measurements with microstructures found to be consisting of equiaxed grains. SEM-BSE images revealed these phases to be present in a duplex microstructure. Tensile tests were performed both at RT and at 500°C. Good tensile properties ($Y_S=546\pm 25$ MPa, $UTS=641\pm 25$ MPa, strain to failure= $2.66\pm 0.65\%$), on-par with or better than traditionally manufactured counterparts, were achieved with excellent strength retention at high temperature in the HIPed condition. The excellent tensile properties at RT were related to the equiaxed duplex microstructures. A summary of these results is presented in Figure 3.11.

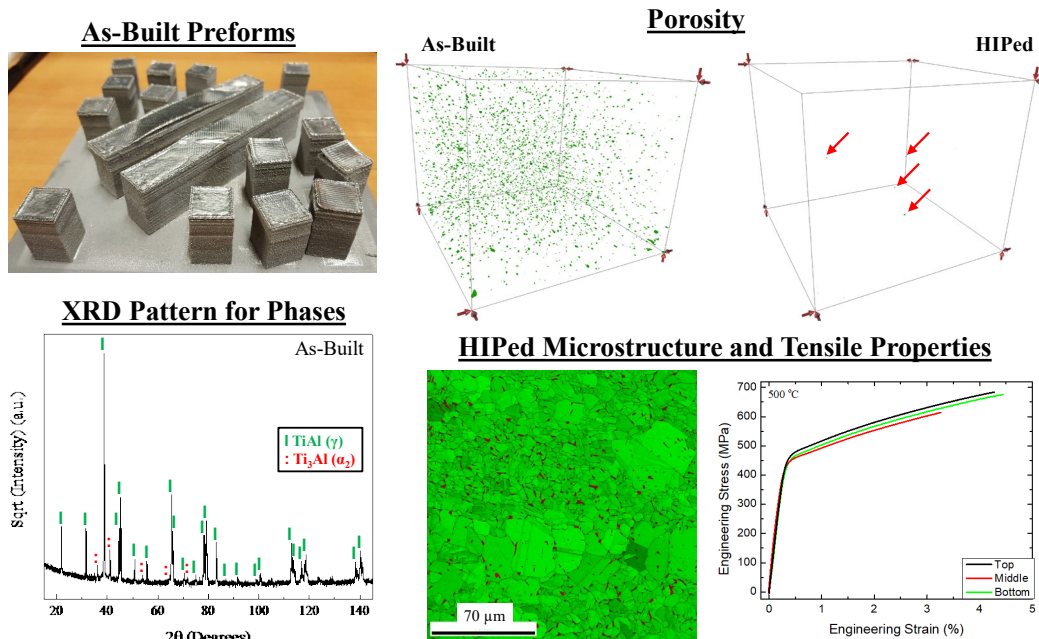


Figure 3.11. A summary figure of the work completed on additive manufacturing of Ti-48Al-2Cr-2Nb (at. %) preforms.

After the proof-of-principle work was successfully established, a CAD model for the turbocharger compressor wheel was obtained from Cummins Inc. A new batch of Ti-48Al-2Cr-2Nb powder was obtained and characterized for morphology and phase identification. Trial runs to print a prototype turbocharger compressor wheel were initiated and continued for 2 weeks. However, these builds failed due to a phenomenon known as ‘smoking’ and is related to the incomplete sintering of the freshly raked powder. When enough un-sintered powder particles are present, electrical charge builds up. The charged powder particles repel each other, blowing out the excess powder, and hence, the name smoking. When smoking is severe enough, it leads to inconsistent raking and sintering followed by a “chain-smoking” event; ending the build process. Following the discussions with the colleagues at the MDF, the existing powder size distribution was concluded to be the main cause behind the build failure and that a coarser cut of powder was needed. Powder was transported to main campus from MDF and sieved to a -100/+200 mesh size (74-149 μm) distribution which was quantified using a laser diffraction powder size distribution analyzer. The sieved powder size distribution is presented in Figure 3.12 with a mean powder size of 104 μm . Next, the major alloying elements: Ti, Al, Nb and Cr were quantified using wet chemical analysis and the results are presented in Table 3.5. The analysis showed that our powder feedstock is within the theoretical compositional spec of Ti-48Al-2Cr-2Nb in at.%. Prototype printing of components using EBM machines at the MDF will be performed in follow-on work.

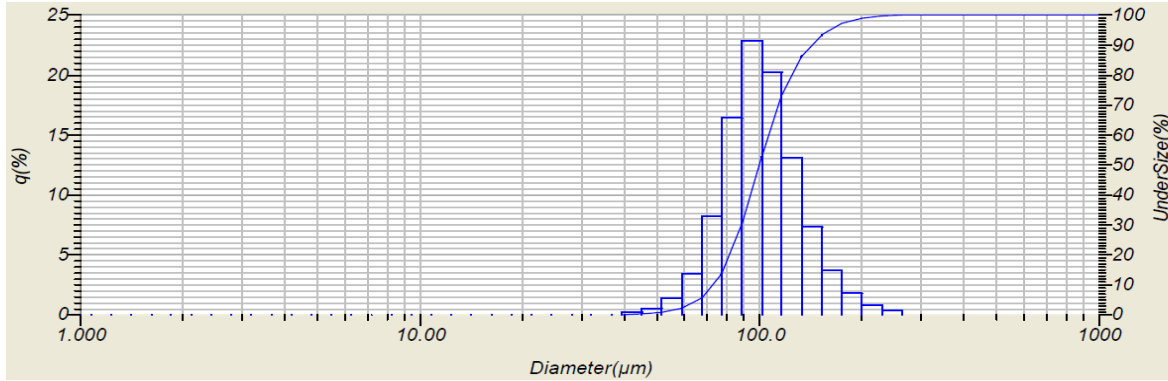


Figure 3.12. The powder particle size distribution of the sieved powder.

Table 3.5. Elemental composition of the Ti-48Al-2Cr-2Nb powder as obtained from wet chemical analysis

Element	Wt. %	At. %
Ti	59.8	48.43
Al	33.2	47.80
Cr	2.54	1.90
Nb	4.45	1.86

Overall, this work has shown that the phase transforming nature of the TiAl alloys enable obtaining equiaxed microstructures in the as-built state without the need for tedious beam parameter manipulations. The HIPed structures have good RT tensile properties that will enable them to be surface machined to the required tolerance that can then be heat treated to obtain the desired microstructures. Additionally, the negligible residual stresses stemming from the high build chamber temperatures ensure the parts are formed without cracks (one of the major issues in traditional manufacturing of these intermetallics).

4. SUBJECT INVENTIONS

No new subject inventions were reported as part of the project.

5. COMMERCIALIZATION POSSIBILITIES

The technologies evaluated in this work are applicable to a wide range of high efficiency diesel engines. It is anticipated that critical technologies such as waste heat recovery will not only demand the availability of improved materials to achieve the efficiency targets for the SuperTruck program in short-term engine efficiency measurements, but will continue to drive the development of advanced materials that would enable the manufacture of a durable, commercially viable high thermal efficiency engine.

6. PLANS FOR FUTURE COLLABORATION

Discussions are currently on-going between ORNL and Cummins for follow-on work on materials for high efficiency engines. There is continued interest in new materials with improved high temperature properties for heads, blocks, exhaust manifolds, pistons, and turbo-charger housings. It is anticipated that additional work will be initiated for the study of various classes of materials relevant to these components in the near future.

7. CONCLUSIONS

This project was successful in evaluating materials that could result in improved temperature capabilities of exhaust manifolds and pistons. The following summarize the accomplishments of this project.

Exhaust Manifold:

- Several candidate alloys to SiMo cast iron were down-selected and constrained thermal fatigue testing was completed to help down-select the best alloys for higher temperature-capable exhaust manifolds
- CF8CP, an ORNL-developed alloy showed the best combination of properties
- A database of thermo-physical and mechanical properties was developed and was provided for thermo-mechanical and lifetime modeling at Cummins
- Prototype two-piece exhaust manifolds were fabricated by MetalTek International- a US based casting house- using new alloy- CF8CP
- New manifolds were tested for endurance for 500 hours in a severe marine cycle and passed the test successfully

Piston Materials

- Multi-layered thermal barrier coatings were deposited on 4140 and Ti-alloy piston materials to evaluate feasibility of better heat-retention in the exhaust gas
- Thermal diffusivities of the composite structures were measured and found to be significantly lower than that of the corresponding base materials.
- Aging of the coatings were performed and thermal diffusivities were measured after the aging treatment
- Thermal cycling evaluations of the composite structure were performed to understand the effect of thermal expansion coefficient mismatch on the performance of the composite during thermal transients and shutdowns
- Microstructural changes in the coatings and the substrate due to thermal cycling were evaluated.

Lubrication evaluation

- Boundary friction and wear behavior of one uncoated and two coated diesel piston skirts were investigated in a base oil without additives, a commercial API CJ-4, and two candidate PC-11 diesel engine oils, as well as in an additive-free basestock.
- One coating has a relatively thick top layer of a polymer-graphite composite and a Mn-P interlayer, while the other coating is a standalone Mn-P film.
- In conformal contact friction tests, there was a 15-30% reduction in friction by the polymer-graphite composite coating compared to the uncoated steel piston but little benefit from the standalone Mn-P coating.

- Changing the oil from CJ-4 to PC-11 had little impact on the friction behavior in boundary lubrication.
- Wear behavior was tested under a point contact configuration with a high contact pressure. The candidate CK-4 oil showed similar or slight better lubricity to the CJ-4 oil while the candidate FA-4 oil decisively increased the piston skirt wear.
- Both coatings prevented scuffing failure observed for the uncoated steel skirt in a base oil without an additive package, they surprisingly caused a higher piston wear rate when tested in any of the fully formulated engine oil. The detrimental impact is attributed to the Mn-P film, either as a standalone coating, or a coating interlayer. The porous and brittle Mn-P film was broken during the wear test and the released hard Mn-P grains are suspected to cause third-body abrasion to accelerate the wear process.

Turbocharger Compressor

- Feasibility of developing an improved high temperature, low mass, cost-neutral turbocharger compressor wheel for heavy-duty engine applications for TiAl using additive manufacturing, utilizing its unique ability to fabricate high strength, low weight structures was evaluated.
- Phase transforming nature of the TiAl alloys enable obtaining equiaxed microstructures in the as-built state without the need for tedious beam parameter manipulations.
- The HIPed structures have good RT tensile properties that will enable them to be surface machined to the required tolerance that can then be heat treated to obtain the desired microstructures.
- Negligible residual stresses stemming from the high build chamber temperatures ensure the parts are formed without cracks (one of the major issues in traditional manufacturing of these intermetallics)

There is continued interest in new materials with improved high temperature properties for heads, blocks, exhaust manifolds, pistons, and turbo-charger housings. It is anticipated that additional work will be initiated for the study of various classes of materials relevant to these components in the near future.

8. REFERENCES

1. P. J. Maziasz, P. J. Shingledecker, N. D. Evans, M. J. Pollard: Developing New Cast Austenitic Stainless Steels with Improved High-Temperature Creep Resistance. *Journal of Pressure Vessel Technology* Vol. 131 / 051404-1 (2009).
2. P. J. Maziasz, B. A. Pint: High-Temperature Performance of Cast CF8C-Plus Austenitic Stainless Steel. *Journal of Engineering for Gas Turbines and Power-Transactions of the ASME* 133 (9), 092102 (2011).
3. J. A. Haynes, B. L. Armstrong, D. Kumar, S. Dryepontd, Y. Zhang: Oxidation of Slurry Aluminide Coatings on Cast Stainless Steel Alloy CF8C-Plus at 800 A degrees C in Water Vapor. *Oxidation of Metals* 80 (3-4), 363-387 (2013).
4. R. I. Pankiw, G. Muralidharan, V. K. Sikka: Development of Stronger and More Reliable Cast Austenitic Stainless Steels (H-Series) Based on Scientific and Design Methodology 2006-06-30, OSTI ID: 886136, ORNL/TM-2006/45 (2006).
5. R. I. Pankiw, G. Muralidharan, V. K. Sikka, P. J. Maziasz: Cast heat-resistant austenitic steel with improved temperature creep properties and balanced alloying element additions and methodology for development of the same, US patent 8,318,083 (Nov 27, 2012).
6. G. Muralidharan, V. K. Sikka, P. J. Maziasz, R. I. Pankiw: Cast, heat-resistant austenitic stainless steels having reduced alloying element content, US Patent US 7,749,432 (Jul 6, 2010).
7. G. Muralidharan, V. K. Sikka, P. J. Maziasz, R. I. Pankiw: Cast, heat-resistant austenitic stainless steels having reduced alloying element content, US Patent 8,003,045 (Aug 23, 2011).
8. G. Muralidharan, Y. Yamamoto, M. P. Brady: Cast alumina forming austenitic stainless steels. US Patent 8,431,072 (April 30, 2013).
9. G. Muralidharan, Y. Yamamoto, M. P. Brady, L. R. Walker, H. M. Meyer III, and D. N. Leonard, "Development of Cast Alumina-Forming Austenitic Stainless Steels," *JOM*, 68 (11), 2803-2810 (2016).
10. D. Li, C. Sloss: Ferrous High-Temperature Alloys for Exhaust Component Applications. *SAE Int. J. Mater. Manuf.*, 3 (1), 391-404 (2010).
11. D. Li, C. Sloss: Amer Foundry: Cast Ferritic Stainless Steels for Automotive Exhaust Components. *Transactions of the American Foundry Society*, Vol 121 121, 487-494 (2013).
12. K. Dawi, J. Favergeon, G. Moulin: High temperature corrosion of the Si-Mo cast iron in exhaust atmosphere. *High Temperature Corrosion and Protection of Materials* 7, Pts 1 and 2 595-598, 743-751 (2008).
13. Y. J. Kim, H. Jang, Y. J. Oh: High-Temperature Low-Cycle Fatigue Property of Heat-Resistant Ductile-Cast Irons. *Metallurgical and Materials Transactions A-Physical Metallurgy and Materials Science* 40A (9), 2087-2097 (2009).
14. Y. L. Yang, Z. Y. Cao, Y. Qi, Y. B. Liu: The Study on Oxidation Resistance Properties of Ductile Cast Irons for Exhaust Manifold at High Temperatures. In: Jiang, Z., Zhang, C.L. (eds.) *Manufacturing Science and Engineering*, Pts 1-5, vol. 97-101. *Advanced Materials Research*, 530-533(2010).
15. K. H. Choe, S. M. Lee, K. W. Lee: High Temperature Oxidation Behavior of Si-Mo Ferritic Ductile Cast Iron. *Materials Science Forum* Vols. 654-656, 542-545 (2010).
16. M. Ekstrom, P. Szakalos, S. Jonsson: Influence of Cr and Ni on High-Temperature Corrosion Behavior of Ferritic Ductile Cast Iron in Air and Exhaust Gases. *Oxidation of Metals* 80(5-6), 455-466 (2013).
17. F. Tholence, M. Norell: High temperature corrosion of cast irons and cast steels in dry air. In: Streiff, R., Wright, I. G., Krutenat, R. C., Caillet, M., Galerie, A. (eds.) *High Temperature Corrosion and Protection of Materials* 5, Pts 1 and 2, vol. 369-3. *Materials Science Forum*, pp. 197-204. (2001).
18. F. Tholence, M. Norell: AES characterization of oxide grains formed on ductile cast irons in exhaust environments. *Surface and Interface Analysis* 34(1), 535-539 (2002).

19. F. Tholence, M. Norell: Nitride precipitation during high temperature corrosion of ductile cast irons in synthetic exhaust gases. *Journal of Physics and Chemistry of Solids* 66(2-4), 530-534 (2005).
20. F. Tholence, M. Norell: High temperature corrosion of cast alloys in exhaust environments I-ductile cast irons. *Oxidation of Metals* 69(1-2), 13-36 (2008).
21. F. Tholence, M. Norell: High temperature corrosion of cast alloys in exhaust environments. II-Cast stainless steels. *Oxidation of Metals* 69(1-2), 37-62 (2008).
22. J. B. Heywood: *Internal Combustion Engines Fundamentals*. McGraw-Hill Mechanical Engineering. ISBN: 9780070286375 (1988).
23. S. R. J. Saunders, M. Monteiro, F. Rizzo: The oxidation behaviour of metals and alloys at high temperatures in atmospheres containing water vapour: A review. *Progress in Materials Science* 53(5), 775-837 (2008).
24. W. J. Quadackers, J. Zurek, M. Hansel: Effect of water vapor on high-temperature oxidation of FeCr alloys. *JOM* 61(7), 44-50 (2009).
25. B. A. Pint, J. P. Shingledecker, M. P. Brady, J. P. Maziasz: *Proceedings of GT2007 ASME Turbo Expo 2007: Power for Land, Sea, and Air May 14–17 (Montreal, Canada, 2007)*, 3, 995-1002 (2007).
26. E. J. Opila: Volatility of common protective oxides in high-temperature water vapor: Current understanding and unanswered questions. In: Steinmetz, P., Wright, I. G., Meier, G., Galerie, A., Pieraggi, B., Podor, R. (eds.) *High Temperature Corrosion and Protection of Materials 6, Part 1 and 2, Proceedings*, vol. 461-464. *Materials Science Forum*, pp. 765-773. (2004).
27. H. Asteman, J. E. Svensson, L. G. Johansson, M. Norell: Indication of chromium oxide hydroxide evaporation during oxidation of 304L at 873 K in the presence of 10% water vapor. *Oxidation of Metals* 52(1-2), 95-111 (1999).
28. M. P. Brady, G. Muralidharan, D. N. Leonard, J. A. Haynes, R. G. Weldon, R. D. England: Long-term Oxidation of Candidate Cast Iron and Stainless Steel Exhaust System Alloys from 650 to 800°C in Air with Water Vapor, *Oxid. Met* 82: 359-381 (2014).
29. A. Shyam, S. Hawkins, D. Erdman, R. England, G. Muralidharan: Constrained thermal fatigue performance of several cast ferrous alloys. *Materials Science Forum*, 783-786, 2388- 2393 (2014).
30. F. Szmytka, P. Michaud, L. Rémy, A. Köster: Thermo-mechanical fatigue resistance characterization and materials ranking from heat-flux-controlled tests. Application to cast-irons for automotive exhaust part, *Int. J. Fatigue* 55, 136-146 (2013).
31. M. B. Grieb, H-J. Christ, B. Plege: Thermomechanical fatigue of cast aluminium alloys for cylinder head applications—experimental characterization and life prediction, *Proc. Eng.* 2, 1767-1776 (2010).
32. A. Constantinescu, E. Charkaluk, G. Lederer, L. Verger: A computational approach to thermomechanical fatigue, *Int. J. Fatigue* 26, 805-818 (2004).
33. S. Amiable, S. Chapuliot, A. Constantinescu, A. Fissolo: A comparison of lifetime prediction methods for a thermal fatigue experiment, *Int. J. Fatigue* 28, 692-706 (2006).
34. R. Gundlach, B. Ross, A. Hetke, S. Valtierra, J. Mojica: Thermal fatigue resistance of hypoeutectic aluminum-silicon casting alloys: *Trans. Amer. Foundrymen's Soc.* 102, 205-224 (1994).
35. H. Wang, G. Muralidharan, D. N. Leonard, J. A. Haynes, W. D. Porter, R. D. England, M. Hays, G. Dwivedi, and S. Sampath: Microstructural Analysis and Transport Properties of Thermally Sprayed Multiple-Layer Ceramic Coatings, *J. Therm. Spray.Tech*, <https://doi.org/10.1007/s11666-017-0680-0>, (2018).
36. R. Miller: *Surface Coating Technology*, vol. 30 (1) pp. 1-11(1987).
37. T. Hejwowski and A. Weronki: *Vacuum*, 2002, vol. 65 (3-4) pp 427-432 (2002).
38. N. P. Padture, M. Gell and E.H. Jordan: *Science*, vol. 296(5566) pp. 280-284
39. Y. J. Su, R. W. Trice, K. T. Faber, H. Wang, W. D. Porter, Thermal conductivity, phase stability, and oxidation resistance of Y₃Al₅O₁₂ (YAG)/Y₂O₃-ZrO₂ (YSZ) thermal-barrier coatings, *Oxidation of Metals* 61 (3-4): 253-271 (2004).
40. S. Ryul Choi, J. W. Hutchinson, A. G. Evans: Delamination of multilayer thermal barrier coatings, *Mechanics of Materials* 31, 431-447 (1999).

41. T. M. Yonushonis,;Overvire of thermal barrier coatings in Diesel Engines, *Journal of Thermal Spray Technology*, Vol. 6(1) pp50-56 (1997).
42. M. Azadi, M. Baloo, G. H. Farrahi and S. M. Mirsalim: A review of thermal barrier coating effects on diesel engine performance and components lifetime, *International Journal of Automotive Engineering*, Vol. 3, No. 1 pp305-317 (2013).
43. A. Levy and S. Macadam: The behavior of ceramic thermal barrier coatings on diesel engine combustion zone components”, *Surface and Coatings Technology*, Vol. 30, pp51-61 (1987).
44. R. Tucker: What Should I Expect from Coating My Engine? *Engine Professional*, Jan-Mar pp34-40 (2010).
45. ASTM Designation E 1461, 933 (2009).
46. W.J. Parker, R. J. Jenkins, C. P. Butler, G. L. Abbott: Thermal Diffusivity Measurements Using the Flash Technique, *J. Appl. Phys.*, 32, 1679-1684 (1961).
47. J. A. Cape, G. W. Lehman: Temperature and Finite Pulse-Time Effects in the Flash Method for Measuring Thermal Diffusivity, *J. Appl. Phys.*, 34, 1909-1913 (1963).
48. R. E. Taylor, L. M. Clark III: Finite Pulse Time Effect in Flash Diffusivity Method, *High Temp. High Press.*, 6, 65-72 (1974)..
49. ASTM Designation E 1269-11, (2011).
50. H. Wang, W. D. Porter, R. B. Dinwiddie: Development of a Thermal Transport Database for Air Plasma Sprayed ZrO₂-Y₂O₃ Thermal barrier Coatings, *Journal of Thermal Spray Technology*, Vol. 19, No. 5, p879 (2010).
51. A. H. Shaw, J. Qu, C. Wang, R. D. England: Tribological study of diesel piston skirt coatings in CJ-4 and PC-11 engine oils. *Wear* 376-377, 1673-1681 (2017).
52. K. Holmberg, P. Andersson, A. Erdemir: Global Energy Consumption Due to Friction in Passenger Cars, *Tribol. Int.*, 47 221–234 (2012).
53. N. Demas, R. Erck, G. R. Fenske: Tribological evaluation of piston skirt/cylinder liner contact interfaces under boundary lubrication conditions, *Lubrication Science* 22, 73-87(2010).
54. K. Nakayama, Y. Yasutake, M. Takiguchi, S. Furuhamas: Effect of piston motion on piston skirt friction of a gasoline engine, *SAE paper*, 970839 (1997).
55. W. Zhang, G. J. Ma, C. W. Wu: Anti-friction, wear-proof and self-lubrication application of carbon nanotubes. *Rev. Adv. Mater. Sci.* 36, 75-88 (2014).
56. S. C. Tung, M. L. McMillan, Automotive tribology overview of current advances and challenges for the future, *Tribology International*, 37(7), 517-536 (2004).
57. Y. Kligerman, I. Etsion, A. Shinkarenko: Improving tribological performance of piston rings by partial surface texturing, *Journal of Tribology* 127, 632-638 (2005).
58. D. Zhu, Y. Hu, H. S. Cheng, T. Arai, K. Hamai: A numerical analysis for piston skirts in mixed lubrication: Part II – Deformation considerations. *Journal of Tribology* 115, 125-133 (1993).
59. K. Patel: *IJEDR*, A review on surface treatment on piston ring and cylinder linear **2(1)**, 1323-1326 (2014).
60. Y. Wang, C. Yao, G. C. Barber, Q. Zou: Scuffing resistance of coated piston skirts run against cylinder bores. *Wear* 259(7-12), 1041-1047 (2005).
61. R. B. Waterhouse, M. Allery: The effect of non-metallic coatings on the fretting corrosion of mild steel, *Wear*, **8** (1965) 112-120.
62. A. Kozłowski, W. Czechowski, Wear resistance of manganese phosphate coatings, *Electrodeposition and Surface Treatment* 3, 55-63 (1975).
63. J. Perry, T. S. Eyre: The effect of phosphating on the friction and wear properties of grey cast iron. *Wear* 43(2), 185-197 (1977).
64. M. Khaleghi, D. R. Gabe, M.O.W. Richardson: Characteristics of manganese phosphate coatings for wear-resistance applications. *Wear* 55, 277-287 (1979).
65. P. Hivart, B. Hauw, J. P. Bricout, J. Oudin: Seizure behavior of manganese phosphate coatings according to the process conditions. *Tribology International* 8, 561-570 (1997).

66. P. Hivart, B. Hauw, J. Crampon, J. P. Bricout: Annealing improvement of tribological properties of manganese phosphate coatings. *Wear* 219, 195-204 (1998).
67. Y. K. Chen, O. P. Modi, A. S. Mhay, A. Chrysanthou, J. M. O'Sullivan: The effect of different metallic counterface materials and different surface treatments on the wear and friction of polyamide 66 and its composite in rolling-sliding contact. *Wear* 255, 714-721 (2003).
68. T. S. N. Sankara Narayanan: Surface pretreatment by phosphate conversion coatings – a review. *Rev. Adv. Mater. Sci.* 9, 130-177 (2005).
69. D. Grimanelis, T. S. Eyre: Wear characteristics of a diffusion bonded sintered steel with short term surface treatments. *Wear* 262, 93-103 (2007).
70. J. D. B. De Mello, H. L. Costa, R. Binder: Friction and wear behavior of steam-oxidized sintered iron components coated with manganese phosphate. *Wear* 263, 842-848 (2007).
71. M. T. Devlin, T. L. Turner, K. Thompson, K. Kolakowski, K. Garelick, J. M. Guevremont T.-C. Jao: Effect of phosphate coatings on fatigue and wear. *NLGI 74th Annual Meeting Scottsdale, Arizona*, (2007).
72. S. Ilaiyavel, A. Venkatesan: The wear behavior of manganese phosphate coatings applied to AISI D2 steel subject to different heat treatment processes. *Procedia Eng.* 38, 1916-1924 (2012).
73. J. Zhang, H. Li: Influence of manganese phosphating on wear resistance of steel piston material under boundary lubrication condition. *Surface & Coatings Technology* 104, 530-536 (2016).

APPENDIX A. PUBLISHED PAPERS

APPENDIX A. PUBLISHED PAPERS

Long-Term Oxidation of Candidate Cast Iron and Stainless Steel Exhaust System Alloys from 650 to 800 °C in Air with Water Vapor

M. P. Brady · G. Muralidharan · D. N. Leonard ·
J. A. Haynes · R. G. Weldon · R. D. England

Received: 23 May 2014 / Revised: 4 August 2014 / Published online: 29 August 2014
© Springer Science+Business Media New York 2014

Abstract The oxidation behavior of candidate cast irons and cast stainless steels for diesel exhaust systems was studied for 5,000 h at 650–800 °C in air with 10 % H₂O. At 650 °C, Ni-resist D5S exhibited moderately better oxidation resistance than did the SiMo cast iron. However, the D5S suffered from oxide scale spallation at 700 °C, whereas the oxide scales formed on SiMo cast iron remained relatively adherent from 700 to 800 °C. The oxidation of the cast chromia-forming austenitics trended with the level of Cr and Ni additions, with small mass losses consistent with Cr oxy-hydroxide volatilization for the higher 25Cr/20–35Ni HK and HP type alloys, and transition to rapid Fe-base oxide formation and scale spallation in the lower 19Cr/12Ni CF8C plus alloy. In contrast, small positive mass changes consistent with protective alumina scale formation were observed for the cast AFA alloy under all conditions studied. Implications of these findings for exhaust system components are discussed.

Keywords Water vapor · Exhaust · Cast iron · Austenitic · Oxidation

Introduction

Silicon–molybdenum (SiMo) cast irons are widely used for exhaust components, such as manifolds and turbocharger housings, in automotive and heavy duty truck diesel engine applications [1–6]. Increased operating temperatures and improved thermal management are expected to enable significant increases in power density,

M. P. Brady (✉) · G. Muralidharan · D. N. Leonard · J. A. Haynes
Oak Ridge National Laboratory, Oak Ridge, TN 37831-6115, USA
e-mail: bradymp@ornl.gov

R. G. Weldon · R. D. England
Cummins Inc., Box 3005, Columbus, IN 47202-3005, USA

Microstructural Analysis and Transport Properties of Thermally Sprayed Multiple-Layer Ceramic Coatings

Hsin Wang¹ · Govindarajan Muralidharan¹ · Donovan N. Leonard¹ · J. Allen Haynes¹ · Wallace D. Porter¹ · Roger D. England² · Michael Hays² · Gopal Dwivedi³ · Sanjay Sampath³

Submitted: 30 August 2017 / in revised form: 3 October 2017
© ASM International 2018

Abstract Multilayer, graded ceramic/metal coatings were prepared by an air plasma spray method on Ti-6Al-4V, 4140 steel and graphite substrates. The coatings were designed to provide thermal barriers for diesel engine pistons to operate at higher temperatures with improved thermal efficiency and cleaner emissions. A systematic, progressive variation in the mixture of yttria-stabilized zirconia and bondcoat alloys (NiCoCrAlYHfSi) was designed to provide better thermal expansion match with the substrate and to improve thermal shock resistance and cycle life. Heat transfer through the layers was evaluated by a flash diffusivity technique based on a model of one-dimensional heat flow. The aging effect of the as-sprayed coatings was captured during diffusivity measurements, which included one heating and cooling cycle. The hysteresis of thermal diffusivity due to aging was not observed after 100-h annealing at 800 °C. The measurements of coatings on substrate and freestanding coatings allowed the influence of interface resistance to be evaluated. The microstructure of the multilayer coating was examined using scanning electron microscope and electron probe microanalysis.

Keywords TBC · thermal barrier coatings · thermal diffusivity

✉ Hsin Wang
wangh2@ornl.gov

¹ Oak Ridge National Laboratory, Oak Ridge, TN 37831, USA

² Cummins Inc., Columbus, IN, USA

³ SUNY Stony Brook, Stony Brook, NY, USA

Introduction

Ceramics coatings have long been used as thermal barriers for aircraft and automobile engines operating at high temperatures (Ref 1, 2). Thermal barrier coatings (TBCs) allow the engine gas temperatures to significantly exceed the limits of traditional alloys or steels, which benefits engine efficiency, and in some cases, emissions (Ref 3). Many studies have focused on lowering thermal conductivity of the coatings, while still maintaining good thermomechanical integrity (Ref 4, 5). Besides lowering thermal conductivity by doping heavy elements for phonon scattering, multiple-layer TBCs have been used to increase interface scattering of the phonons and oxidation resistance (Ref 5). For example, alternate YSZ and YAG layers were used to promote interface scattering (Ref 4).

Initial applications of TBCs on diesel engines were carried out using a Cummins V903 direct injection engine under DOE/NASA and TACOM programs (Ref 6) focusing on cylinder head and piston coatings. The TBC is designed as a thermal shield, with the goal of ultra-low thermal conductivity. However, this reduced thermal conductivity can also be a source of high thermal stresses, particularly in thicker coatings. Although TBCs have been used to protect internally cooled stationary and rotating hot section components in aero engines and land-based turbines for decades, introduction of TBCs into high-volume reciprocating engines has been a very slow process due to the extreme conditions on the piston crown surface and the very long service lives of heavy duty diesel engines prior to first overhaul (Ref 6-8). On the other hand, TBCs have been widely used in race car engines in which short-term performance is more important than long-term durability (Ref 9). Improving the thermomechanical properties of the TBC



Case study

Tribological study of diesel piston skirt coatings in CJ-4 and PC-11 engine oils

Austin H. Shaw^a, Jun Qu^{a,*}, Chinpei Wang^b, Roger D. England^b^a Materials Science and Technology Division, Oak Ridge National Laboratory, P.O. Box 2008, MS-6063, Oak Ridge, TN 37831-6063, USA^b Technical Center, Cummins, Inc, USA

ARTICLE INFO

Article history:

Received 25 August 2016

Received in revised form

11 January 2017

Accepted 20 January 2017

Keywords:

Diesel piston skirt

Friction

Wear

PC-11 engine oil

Manganese phosphate

Polymer-graphite coating

ABSTRACT

Piston skirt coatings are used in heavy-duty diesel engines for reduction of friction, noise, and scuffing. This study explored the friction and wear behavior of two piston skirt coatings, a polymer-graphite composite coating with a manganese phosphate (Mn-P) interlayer and a standalone Mn-P coating, in API CJ-4 and candidate PC-11 (CK-4 and FA-4) diesel engine oils. Two test configurations were used: conformal contact similar to that in an actual engine to examine the friction behavior under normal operating conditions, and point contact to study the wear performance under extreme pressure conditions. Results suggest that CK-4 could replace CJ-4 without wear penalty but FA-4 may post a potential wear challenge. The standalone Mn-P coating showed little friction benefit in the conformal contact, but made a detrimental impact on wear performance of the piston skirt in the point contact. It is hypothesized that the hard Mn-P grains worn off the coating acted as abrasive at the sliding interface to promote third-body abrasion accelerating the material removal. The polymer-graphite composite coating reduced the friction by 15–30% in the conformal contact tests in the three engine oils. However, in the point contact sliding, the polymer-graphite coating caused a higher wear rate, which is attributed to the Mn-P interlayer releasing hard particles after the top coat was worn through.

© 2017 Elsevier B.V. All rights reserved.

1. Introduction

Roughly 10–15% of total energy generated in an internal combustion engine is lost to parasitic friction [1]. In the piston-cylinder assembly, while the piston rings may account for more than 70% of the total friction-induced energy losses [2], the piston skirt's contribution to the friction of the system could also be substantial [3–5] and should not be overlooked. Others stressed that the friction between the piston skirts and cylinder walls could even be comparable in magnitude to the friction between the rings and the cylinder walls in certain circumstances [6,7]. Coating the piston skirts [8,9] is among the materials approaches for reduction of friction, noise, and scuffing, particularly to address the increasing peak-cylinder-pressure and decreasing oil viscosity in heavy-duty diesel engines.

Manganese phosphate (Mn-P) coatings have been used in the industry for more than half a century for anti-scuffing/anti-seizure and wear protection in both dry and lubricated environments, but the literature on their tribological behavior is surprisingly limited, with only a little more than a dozen of reports found in our survey [10–22]. In this work, three diesel piston skirts, one uncoated steel, another coated with a standalone Mn-P film, and the third coated

with a polymer-graphite composite layer on top of a Mn-P interlayer, were tribologically investigated in lubrication of a commercial API CJ-4 as well as two candidate PC-11 diesel engine oils.

2. Experimental and materials

Three diesel pistons were provided by Cummins: (1) uncoated 38MnSiV5S steel, (2) skirt coated with a Mn-P film, and (3) skirt coated with a polymeric matrix containing colloidal graphite short fibers and a Mn-P interlayer (henceforth referred to as polymer-graphite coating). The photographs of the three pistons are shown in Fig. 1. The Mn-P conversion coating or interlayer was produced by immersion in a dilute solution of phosphoric acid and manganese phosphate salts that chemically react with the steel piston surface to form a layer of crystalline phosphates. The Mn-P coating contains a small amount of iron phosphates and the coating composition may be expressed as $(\text{Mn}^{2+}, \text{Fe}^{2+})_x[\text{PO}_3(\text{OH})\text{PO}_4]_2 \cdot 4\text{H}_2\text{O}$. The amount of iron generally is rather low (<5%) and varies depending on the process parameters. The polymer-graphite composite coating was applied to the piston skirt surface using screen print followed by a curing process. The polymer-graphite coating consists a PAI (polyamide-imide) matrix embedded with 10–20 wt.% short graphite fibers (<2 μm long). A mating grey cast iron cylinder liner from Cummins, as shown in Fig. 1d, was used as the counterface material

* Corresponding author.

E-mail address: qujn@ornl.gov (J. Qu).<http://dx.doi.org/10.1016/j.wear.2017.01.082>

0043-1648/© 2017 Elsevier B.V. All rights reserved.

Constrained thermal fatigue performance of several cast ferrous alloys

Amit Shyam^{1,a}, Shane Hawkins^{1,b}, Donald Erdman^{1,c}, Roger England^{2,d}
and Govindarajan Muralidharan^{1,e}

¹Oak Ridge National Laboratory, 1 Bethel Valley Road, Oak Ridge, TN 37831, USA

²Cummins Inc, 1900 McKinley Avenue, Columbus, IN 47201, USA

^ashyama@ornl.gov, ^bhawkinscs@ornl.gov, ^cerdmandl@ornl.gov,
^droger.d.England@cummins.com, ^emuralidhargn@ornl.gov

Keywords: Constrained thermal fatigue; cast ferrous alloys; plasticity; modeling.

Abstract. An experimental setup that was utilized to evaluate the constrained thermal fatigue (CTF) behavior of several cast ferrous alloys is described. The tests performed allowed the assessment of the relative performance of different materials in CTF loading. The stable hysteresis loop of the individual CTF tests further allowed the development of a unified parameter that determined the level of inelastic (plastic and creep) deformation and the CTF life under those conditions. A CTF life prediction methodology for cast ferrous alloys is outlined.

Introduction

Constrained thermal fatigue (CTF) is a common cause of failure in automotive and heavy duty diesel engine components. CTF loading involves cycling of temperature superimposed on mechanically constrained components such as exhaust manifolds and engine cylinder heads [1]. While models to determine the isothermal low cycle fatigue performance are well established (e.g. Coffin-Manson model), similar models for constrained thermal fatigue are material specific and invariably require extensive numerical and finite element computations [1-4]. Direct evaluation and ranking of the constrained thermal fatigue performance of materials, moreover, remains a challenge [5].

A setup was developed to evaluate the constrained thermal fatigue performance of alloys. This setup was utilized to compare and rank the CTF performance of six cast ferrous alloys. It will be shown that a parameter derived from the stable hysteresis loop can be used to unify the plastic and creep deformation under those conditions. The CTF life for the six ferrous alloys can also be well predicted with this unified inelastic parameter.

Experimental Procedure

The test specimens were rigidly constrained in this testing methodology, in a servohydraulic test machine in displacement control (Fig. 1), and cyclic stresses were generated by temperature cycling in the gage section of the specimen between specified temperatures and at a specified heating rate. Heating of specimens was achieved by combining several resistance heaters. In addition, a hold time at the maximum temperature in the cycle was introduced to generate a trapezoidal temperature versus time control signal. All the reported tests in the present investigation had a maximum temperature of 800°C and hold time at maximum temperature of 60 seconds. Heating/cooling rates of 1°C/second were employed in the reported tests with a feedback loop temperature controller (with Proportional Integrative Derivative, PID control). Precise temperature control (less than 5°C variation) in the gage section of the specimen was achieved by a Labview® software code. A high temperature extensometer was placed in the gage section of the specimen and the evolution of the stress and strain signals with thermal cycling was continuously recorded. The specimens were cycled to failure. The fracture surface of selected specimens was examined by scanning electron microscopy (SEM).